https://doi.org/10.26599/FRICT.2026.9441219

Research Article

Atomic insights of material removal mechanism in chemical mechanical polishing for silicon using developed abrasive-free slurry

Lei Chen[a,*] ✉, Shehui Dang[a,*], Jinhuan Zhong[b], Chen Xiao[a,b], Yang Wang[b], Lifei Zhang[c], Yilong Jiang[a], Linmao Qian[a],

* Lei Chen and Shehui Dang contributed equally to this work.

[a]*Tribology Research Institute, State Key Laboratory of Rail Transit Vehicle System, School of Mechanical Engineering, Southwest Jiaotong University, Chengdu 610031, China*

[b]*Research Institute of Frontier Science, Southwest Jiaotong University, Chengdu, 610031, China*

[c]*State Key Laboratory of Tribology in Advanced Equipment, Tsinghua University, Beijing, 100084, China*

✉ E-mail: chenlei@swjtu.edu.cn (L. C.)

Received: November 26, 2025; Revised: December 28, 2025; Accepted: January 26, 2026

Abstract

Atomic surface of silicon (Si) wafers without particulate contamination achieved by chemical mechanical polishing (CMP) is highly desired for advanced chip manufacturing. Traditional CMP processes usually employ abrasive-containing slurries, resulting in significant particulate residues and high-cost post-treatments. To settle this challenge, a novel abrasive-free CMP slurry only including designated chain-length alkylamine was developed based on the observed dependence between the Si surface roughness and alkylamine chain length. After polishing by the long-chain hexylamine slurry, an atomic surface without particulate contamination is achieved with surface roughness as low as 0.13 nm, which is 85% lower than that obtained using short-chain methylamine slurry, while maintaining a material removal rate of 57.7 nm/min. Then, we established an atomic mechanistic framework that integrates interfacial chemistry with mechanical action to understand how alkylamine chain length modulates mechanochemistry in abrasive-free Si CMP. Density functional theory calculations show that long-chain alkylamines adsorb more readily but have a milder weakening effect on Si–Si bonds, whereas short-chain counterparts, despite weaker adsorption, more effectively weaken these bonds. Nanowear tests and X-ray photoelectron spectroscopy corroborate that the dynamic equilibrium between the adsorption strength and bond weakening promotes the formation of a mechanically vulnerable reaction layer composed by O_x–Si–N_y compounds amenable to abrasive-free removal for atomic smoothness. Our findings shift the mechanistic paradigm from conventional abrasive-involved interfacial interactions to abrasive-free, chemically driven, adsorption-controlled removal processes. These insights offer valuable theoretical guidelines for both academic research and industrial practice in ultra-precision manufacturing and

advanced semiconductor processing.

Keywords: Chemical mechanical polishing; Interfacial mechanochemistry; Abrasive-free removal; Atomic surface; Alkylamine; Silicon

1. Introduction

Chemical mechanical polishing (CMP), a process extensively employed in integrated circuit (IC) manufacturing, utilizes chemical additives and abrasives incorporated into slurries to regulate its performances, thereby achieving global planarization across wafer-scale surface [1-7]. As the feature size of advanced chips shrinks to 5 nm or less, an atomic surface of wafers without particulate contamination is required for advanced semiconductor materials such as silicon (Si) [8-10], diamond [11, 12] and silica [13-15]. In traditional abrasive-containing CMP processes, material removal of wafer relies on abrasive particles that driven by polishing pad to attack wafer surface via complex motion, such as scratching and rolling [16, 17]. Once these particles slide against wafer surface, they are difficult to detach due to mechanochemical interaction, thereby resulting in substantial particulate residues [18]. This not only compromises the reliability of microstructures of ICs, but also necessitates complex and high-cost post-CMP cleaning processes [19]. Therefore, developing abrasive-free CMP process is imperative. For abrasive-free slurries, the surface flatness of wafers is governed by chemical additives, as their molecular structures significantly impact the dynamic equilibrium between mechanical action and chemical reactions in the CMP process [20-22]. However, current mechanistic understanding by which molecular structures of the chemical additives govern the CMP

performances still remains rudimentary due to the complexity of the coupling between mechanical and chemical in practical CMP processes [23, 24], thereby hindering the further improvement of the current CMP processes.

Si has been extensively used as structural and substrate material in the fabrication of over 90% of ICs, underpinning the modern electronics industry [3, 9, 25, 26]. The pursuit of atomic surfaces without particulate contamination remains a persistent challenge in Si CMP, primarily due to its high chemical reactivity [27]. Previous studies have made considerable efforts to focus on the interaction between abrasives and Si surface, among which the most significant advancement is the incorporation of chemically reactive nanoparticles (e.g., ceria or silica) into the slurry to achieve sub-nanometer surface finishing [28, 29]. In these systems, abrasives particles are dynamically driven by the polishing pad to interact with the Si surface, initiating mechanochemical reaction [30, 31]. Here, interfacial bonding bridges formed between Si and abrasive surfaces with the participation of water molecules induce the rupture of Si–Si networks, resulting in the removal of the topmost material layer [27, 32]. However, the chemically active abrasive particles tend to adhere strongly to the Si surface via chemical bonding, which not only complicates the post-CMP cleaning process but also risks damaging the crystalline structure of the Si substrate during particle removal [19, 33]. More critically, the intrinsic interactions between chemical reagents and Si in the dynamic polishing process are largely masked by the dominant effects of abrasive–Si interactions, which results their fundamental mechanisms been relatively overlooked in the most current studies.

For abrasive-free CMP slurries, the polishing performance is dominated by the chemical reagents, with their molecular structures critically shaping the final surface flatness. In

particular, amine-containing compounds are often introduced as accelerators to enhance the material removal rate of Si, as the amine group can weaken Si–Si bonds and render them more susceptible to chemical attack, thereby improving the CMP efficiency [10, 20, 34]. However, variations in the molecular structure of these amines, especially the carbon chain length, can significantly alter the adsorption behavior on the Si surface [35, 36]. Such changes may hinder the ability of these molecules to weaken interatomic bonds, consequently affecting the material removal process and compromising the final surface quality [22, 37]. Despite its significance, most current studies remain empirical observations and fall short of uncovering the fundamental interfacial mechanisms involved. This gap largely stems from the inherent challenges associated with *in situ* characterization of reaction layer formation and removal during CMP [38, 39]. Consequently, the current research offers merely phenomenological insights and lacks the mechanistic understanding of how molecular structure influences the CMP performances that are essential for further improve CMP performance in the manufacturing of high-end chips.

The present study systematically investigates the effect of molecular structure of chemical reagents on CMP performance as a function of carbon chain length and concentration using a homologous series of primary alkylamines, i.e., methylamine (MA), ethylamine (EA), propylamine (PA), butylamine (BA), amylamine (AA), and hexylamine (HA). The mechanical and chemical properties of the polished Si surfaces were characterized by various techniques, including a static etching test, X-ray photoelectron spectroscopy (XPS), and atomic force microscopy (AFM) nanowear test. Furthermore, density functional theory (DFT) calculations were performed to reveal the atomistic mechanisms underlying the interactions between alkylamines and Si surface. Our findings provide useful knowledge for further improving CMP

performance and shed new light for optimizing the design of high-performance slurries.

2. Material and methods

2.1 Experiment method

The abrasive-free CMP process involves alternating chemical and mechanical steps: (1) the formation of a reaction layer forms via chemical reaction between the slurry and Si surface, followed by (2) mechanical removal of this layer via multi-asperity contact with the polishing pad under applied pressure (**Fig. 1**a-c) [40]. To elucidate the underlying removal mechanism in CMP, the inherently complex and stochastic multiple-asperity contact was simulated by precisely controlling sliding parameters in single-asperity contact using AFM at the nanoscale (**Fig. 1**d and e) [17]. To further clarify the interaction reaction mechanism between the alkylamines and Si surface, the reaction process was simulated by performing DFT calculations at atomic scale (**Fig. 1**f). By bridging nanoscale interfacial chemistry and mechanical action, the underlying mechanism of Si removal during dynamic CMP process was systematically revealed.

2.2 Polishing experiments

P-doped Si wafer with a diameter of 50.8 mm was supplied by Jingxin electronics technology Co., Ltd., Suzhou, China. Prior to CMP, wafers were dipped in 3 wt% HF solution for 2 min to remove native oxide layers. The components of the CMP slurries are shown in **Table 1**. CMP experiments were performed by an automatic pressure polisher (UNIPOL-1200S, Shengyang Kejing Auto-instrument Co., Ltd, China) using the polishing parameters listed in

Table 2. The material removal rate (MRR) was calculated by measuring the mass difference before and after polishing using a Sartorius ME36S microbalance with a readability of 1 μg. After each polishing, the polishing pad is conditioned for 60 s with a diamond grit pad.

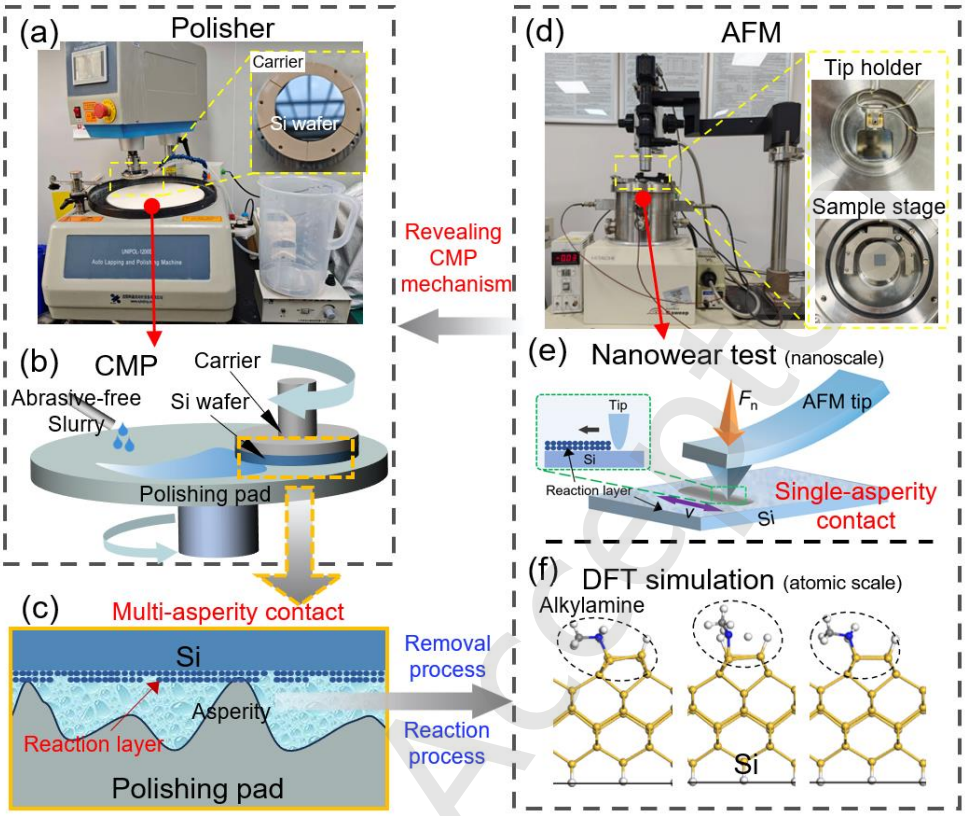

Fig. 1 Schematic representation of the multiscale material removal mechanism in Si CMP. (a) Photograph of automatic pressure polisher. (b) Material removal dominated by the multi-asperity-contact (c) in CMP process at macroscale. (d) Photograph of the AFM used in the nanowear tests. (e) Mechanical removal in the CMP simulated by single-asperity-contact in AFM tests at nanoscale. (f) DFT calculation of the reaction process at atomic scale.

Table 1 Abrasive-free slurry components used in this study.

	Chemical agents	pH	Water
Content	0~100 mM alkylamines	10	Balance

Source	TCI Development Co., Ltd.	Adjusted with KOH and HNO_3	Master-S15, Hitech Instruments Co., Ltd.

Table 2 CMP parameters for polishing Si wafers.

Parameters	Value
Polishing pad	IC1010/Sub IV
Carrier/platen speed	80/90 rpm
Slurry flow rate	100 ml/min
Polishing time	3 min
Down pressure	3.5 psi

2.3 Characterization

The chemical reactivity of alkylamines toward the Si surface was assessed via static etching experiments where the Si wafers were immersed in designated slurries for 1.5 min. The static etching rate (SER) was calculated based on weight loss measurements using a Sartorius ME36S microbalance. The elemental compositions of Si wafers were characterized by X-ray Photoelectron Spectroscopy (XPS, AXIS Ultra DLD, Kratos Analytical). The mechanical properties of the wafers were estimated via an AFM (SPI3800N, Seiko, Japan) by sliding against with a chemically inert diamond tip (NC-LC, Adama, Ireland, curvature radius of 20 nm) to exclude chemical contributions. The nanowear tests were conducted under the following conditions: sliding velocity of 2.4 μm/s, number of reciprocating cycles of 20, applied loads F_n of 1.5 μN, and a sliding stroke D of 0.6 μm. The topographies of the nanoscratches and wafer surfaces were imaged using a sharp Si_3N_4 tip. Additionally, the zeta potentials of Si

nanoparticles (diameter of 60 nm) in the designated slurries were measured using a zeta potential analyzer (Zetasizer Nano ZS, Malvern Instruments, UK).

2.4 Theoretical simulation details

2.4.1 Basic setup of DFT calculation

Geometric optimization was carried out using the Dmol^3 module [41] in the Materials Studio software. The generalized gradient approximation (GGA) functional with the Perdew-Burke-Ernzerhof (PBE) exchange-correlation and DNP basis set were employed [42]. The k-points mesh precision was set to 2×1×1, and the self-consistent field (SCF) convergence tolerance was set to 1.0×10^{-6} eV/atom. The conductor-like screening model (COSMO) with a dielectric constant of water (ε_{water} = 78.54) was introduced to simulate the aqueous environment [43]. To account for van der Waals interactions, Grimme's DFT-D correction was applied [44, 45]. The computational model is based on a Si(100) 2×4 model, designed to eliminate interatomic interactions in the xy direction. The Si surface is reconstructed and passivated with hydrogen atoms, while the bottom two silicon layers are fixed. A vacuum layer of 15 Å is introduced, and a total of five Si layers are used for surface reaction calculations.

2.4.2 Transition state search

Transition state search was performed using the Dmol^3 module with the Complete LST/QST protocol [46], setting the task type to TS Search. The optimized option of reactants and products was selected to ensure reactants and product structures were minimized. Transition state verification was verified by vibrational frequency analysis, with the presence of a single frequency confirming that the structure corresponds to a first-order saddle point on the potential

energy surface.

2.4.3 Calculation of force constant

To evaluate changes in chemical bond strength within Si systems, local vibrational mode analysis based on Cremer-Konkoli theory was employed [47]. Using Vienna Ab-Initio Simulation Package (VASP), Phonopy, and LModeA-nano plugin [48], force constants were calculated in a Si cluster model to reduce computational complexity [49]. The cluster model can accurately capture the local interfacial interactions, including force constants and charge distributions at surface active sites, and its validity has been extensively demonstrated in previous studies [50, 51]. The plane-wave basis set kinetic energy cutoff was set to 400 eV. First, the basic parameters were set. The VASP calculation parameters were kept consistent with those in Materials Studio (EDIFF = 1E-06, EB_K = 78.54), and geometric optimization was performed on the Si cluster model. After completing the structural relaxation, the vibration frequencies are calculated using VASP and the results are stored in the vasprun.xml output file. The Hessian matrix is then extracted from this file using Phonopy, and in combination with the LModeA nano plugin, the local mode force constants are computed to achieve a quantitative analysis of changes in chemical bond strength.

3. Results and discussion

3.1 Effect of the carbon chain length of alkylamines on the CMP performance of Si

A homologous series of primary alkylamines — MA (C_1), EA, (C_2), PA (C_3), BA (C_4), AA (C_5), and HA (C_6) — were selected as key chemical additives for the Si CMP experiments. As

illustrated in **Fig. 2**a, all compounds share a common molecular architecture, featuring a terminal primary amine group ($–NH_2$) connected to linear alkyl chains ranging from methyl (C_1) to hexyl (C_6). This series provides a model system for systematically investigating how the molecular structure, particularly the carbon chain length, influences CMP performance.

The effects of these six alkylamines on Si CMP performance were examined across a range of concentrations. As shown in **Fig. 2**b, the MRR for short-chain alkylamines (C_1–C_2) increases monotonically with concentration. In contrast, for medium-chain alkylamines (C_3–C_4), MRR increases linearly at low concentration regime (0-25 mM) but plateaus at high concentrations (>25 mM). For long-chain alkylamines (C_5–C_6), MRR reaches a maximum at 10 mM and then decreases significantly at higher concentrations (**Fig. 2**b). At 10 mM (**Fig. 2**c), the MRR shows a positive correlation with carbon chain length, increasing by 21% from ~306.1 nm/min (C_1) to 369.0 nm/min (C_6). However, at 100 mM (**Fig. 2**c), the trend reverses dramatically: MRR decreases by ~90% with increasing carbon chain length, dropping from ~555.0 nm/min (C_1) to 57.7 nm/min (C_6). The pronounced variations in MRR likely stem from the synergistic effects of carbon chain length and concentration, implying a shift in the underlying interaction mechanism between alkylamines and Si in the CMP process.

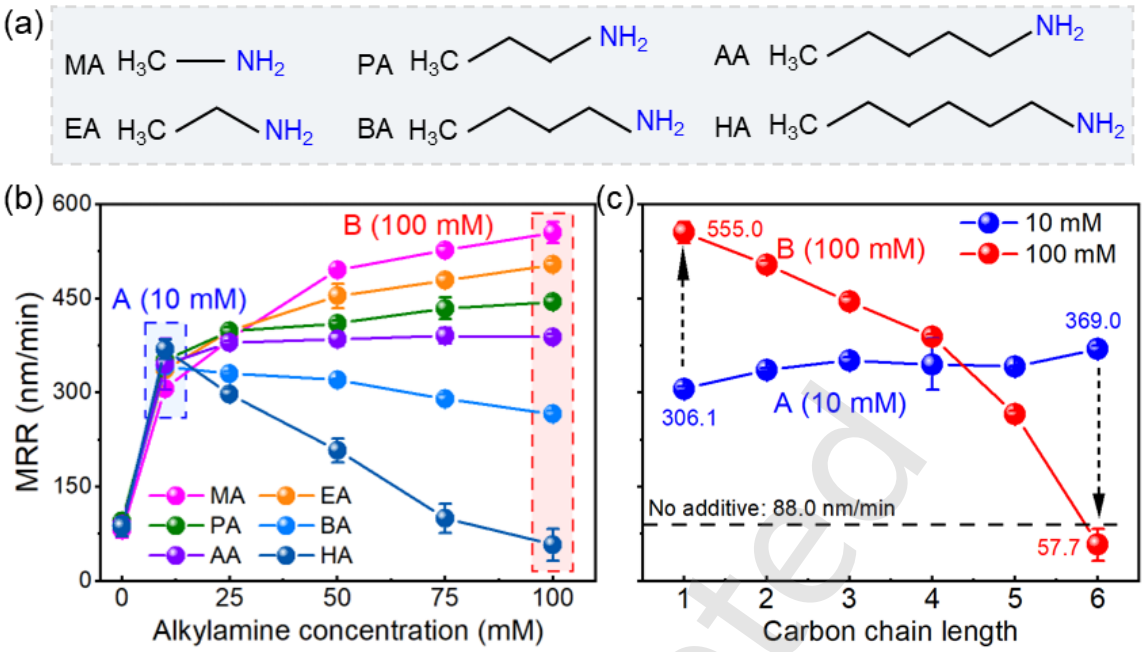

Fig. 2 Effect of the six alkylamines on the MRR of Si in the CMP tests. (a) Schematic molecular structures of the six alkylamines: MA (C_1), EA (C_2), PA (C_3), BA (C_4), AA (C_5), HA (C_6). (b) MRR as a function of the concentration of the alkylamines. (c) MRR as a function of carbon chain length. The MRR data (10 and 100 mM) in (c) corresponds to the regions highlighted by the blue and red rectangular boxes in (b).

Fig. 3 presents the S_a and the peak-to-valley (PV) value of Si after CMP with the designated alkylamine-based slurries, while **Fig. 4** displays the representative AFM topographies and cross-section profiles. Both S_a and PV values decrease with increasing carbon chain length at alkylamine concentrations of 10 mM and 100 mM, indicating improved surface quality with longer-chain alkylamines. This trend is more pronounced at 100 mM, where the reduction in S_a and PV values is nearly 84% and 79%, respectively, from C_1 to C_6, ultimately achieving an atomic-level smooth Si surface. Specifically, at 10 mM, S_a/PV values decrease from 0.35 nm/3.9 nm (C_1) to 0.25 nm/2.5 nm (C_6). At 100 mM, S_a/PV values decrease from 0.84 nm/7.5 nm (C_1) to 0.13 nm/1.6 nm (C_6). Increasing the alkylamine chain length serves as a bridge to effectively

balance the mechanical and chemical interactions in the dynamic polishing process, enabling controlled MRR and ultimately obtaining an atomic-level smooth surface (**Fig. 5**). Although using the slurry containing 100 mM HA(C_6) leads to an approximately 90% reduction in MRR compared to the slurry containing 100 mM MA(C_1), it enables the achievement of an atomic-level smooth surface without particulate contamination. Such surface quality is crucial for improving performance and product yield of ICs, and the reduced MRR can be acceptable in some cases (e.g. Si surface used for lithography or ion implantation) [52]. The above results underscore the critical interplay between chain length and concentration in governing both material removal efficiency and surface quality, suggesting that fine-tuning these parameters is essential for optimizing the CMP process in advanced chip manufacturing.

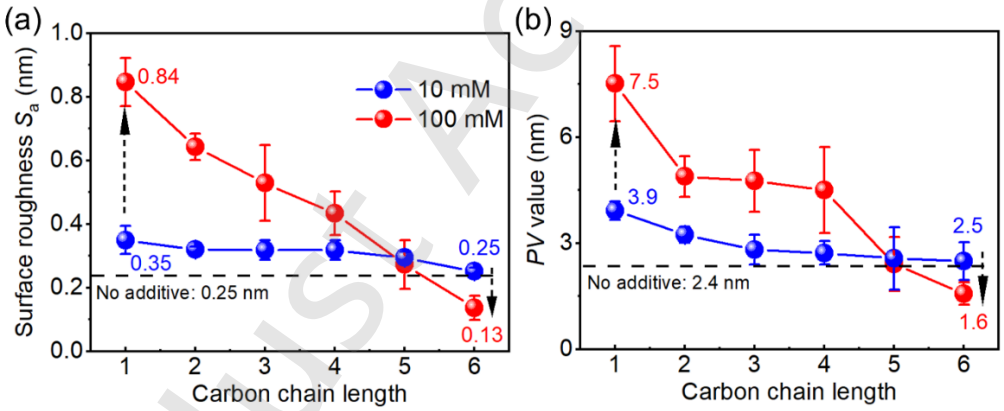

Fig. 3 Carbon chain length and concentration effects of the alkylamines on the surface quality of Si in the CMP tests. (a) S_a. (b) *PV* value.

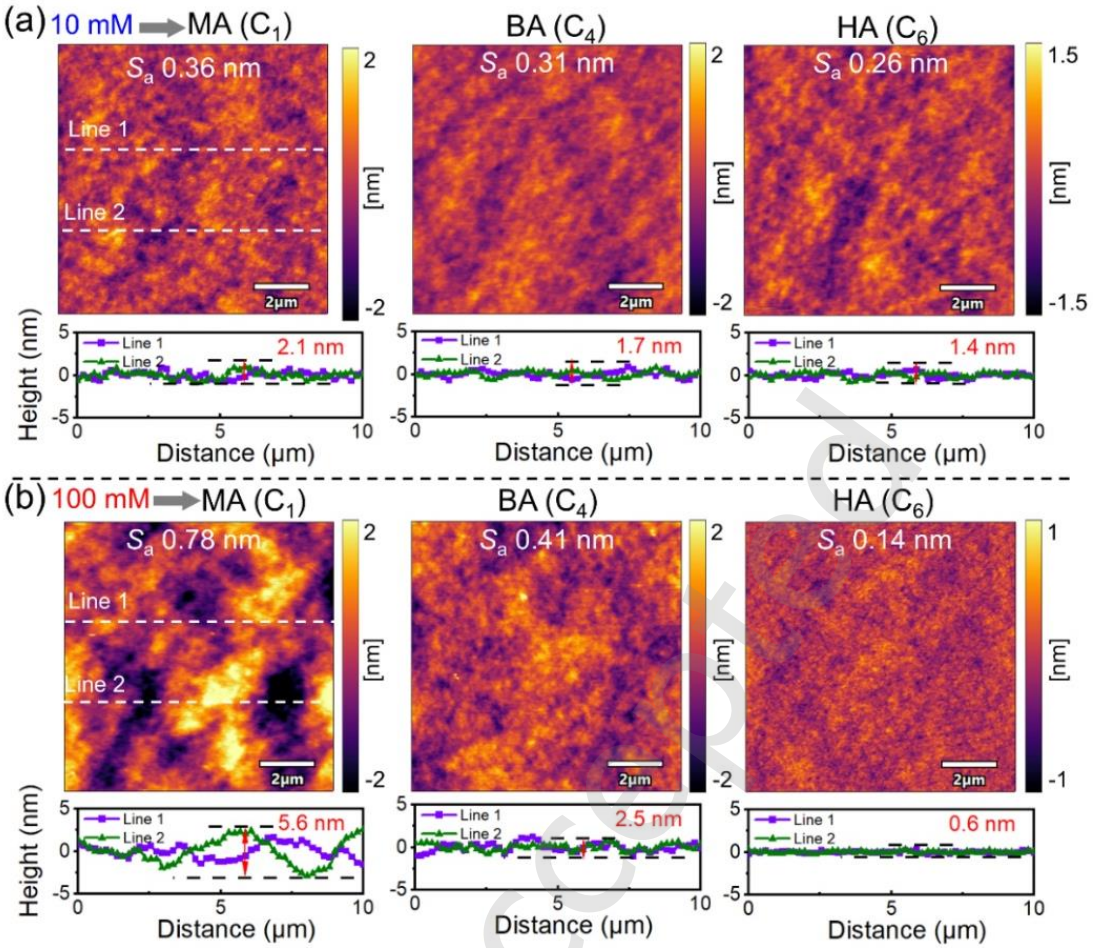

Fig. 4 Typical AFM topographies (top) and cross-section profiles (bottom) of Si after polishing with the slurries containing the 10 mM (a) or 100 mM (b) alkylamine (MA, BA and HA).

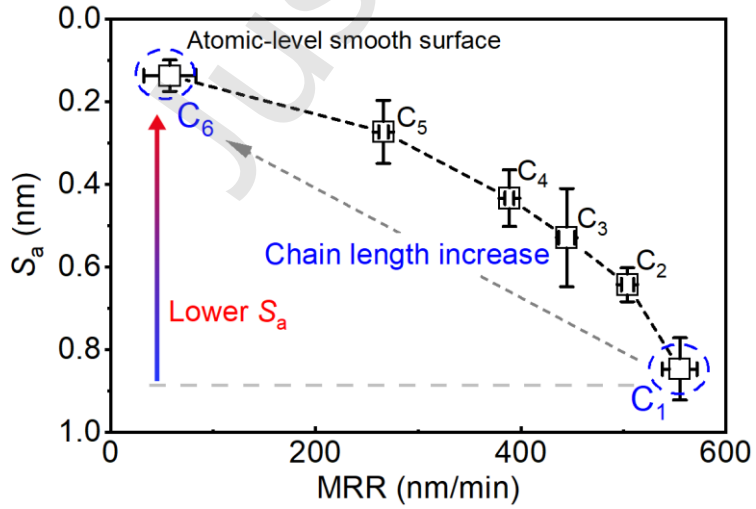

Fig. 5 S_a as a function of MRR at 100 mM alkylamine (C_1~C_6). Increasing the chain length of

alkylamines provides an effective means to modulate the CMP performances.

3.2 Chain-length dependent chemical interactions between alkylamines and Si

To evaluate the chemical reactivity of the six alkylamines, static etching experiments were conducted. **Fig. 6** presents the S_a values of Si surfaces (1×1 μm) etched with the designated alkylamine-based slurries and the corresponding SER, while **Fig. 7** displays the representative AFM images and cross-sectional profiles of the etched Si surfaces. At 10 mM, all etched Si surfaces exhibit minimal topographical change with no visible corrosion pits. In contrast, at 100 mM, significant corrosion occurs on MA (C_1)-etched surface, forming a rough surface with a S_a of 1.51 nm. This indicates that MA at high concentration exhibits strong chemical aggressiveness, thereby damaging the integrity of Si surface, as evidenced by the presence of numerous nanoscale corrosion pits on the surface. With increasing carbon chain length, both the number of corrosion pits and S_a gradually decrease, particularly on the HA (C_6) etched surface, which shows a near-pristine topography. The SER results (**Fig. 6**b) follow a similar trend to the MRR data (**Fig. 2**c). At 10 mM, the SER increases modestly with chain length, from ~1.3 nm/min (C_1) to ~1.9 nm/min (C_6). In contrast, at 100 mM, SER drops dramatically from ~7.6 nm/min (C_1) to ~-0.2 nm/min (C_6), reflecting a sharp decline in chemical reactivity with increasing chain length. The negative SER observed for HA (C_6) at 100 mM (~-0.2 nm/min) suggests a slight mass gain on the Si surface, likely due to the adsorption of HA molecules.

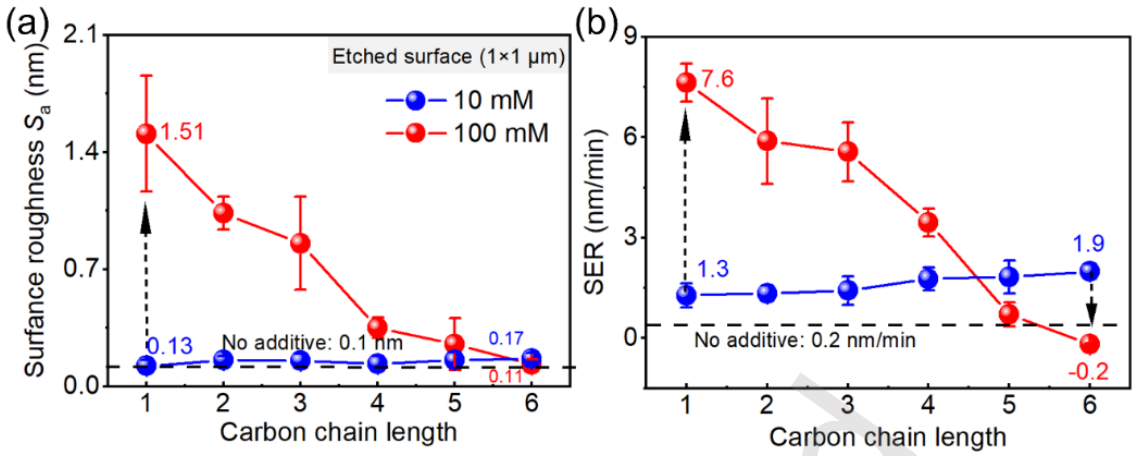

Fig. 6 Carbon chain length and concentration effects of the alkylamines on the static etching experiments of Si. (a) Etched surface roughness S_a. (b) SER.

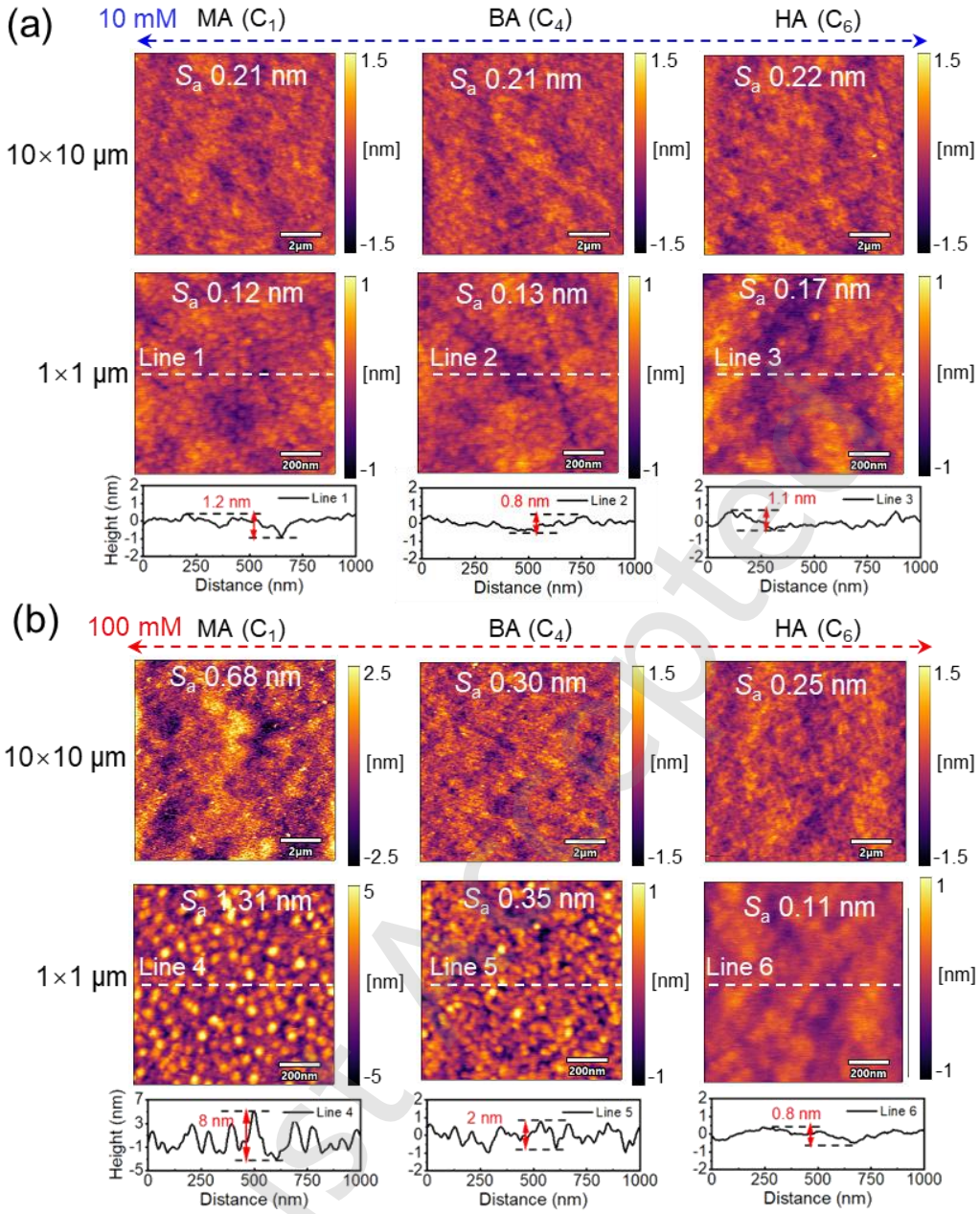

Fig. 7 Typical AFM topographies and cross-sectional profiles of Si after etching with the slurries containing 10 mM (a) or 100 mM (b) alkylamine (MA, BA and HA).

To verify whether the dual-dependent behavior originates from the differences in alkylamines adsorption, the species distributions at pH 10 were calculated. The pKa values for the acidic forms of MA, EA, PA, BA, AA, and HA are 10.66, 10.65, 10.54, 10.60, 10.63, and 10.56, respectively [53]. Using the distribution fraction formula [54], the fractions of the two

species — RNH_2 (neutral) and RNH_3^+ (protonated) — in aqueous solution at pH 10 can be determined, where R represents alkyl group (C_1~C_6). As shown in **Fig. 8**a, the species distribution of six alkylamines remains almost constant, where RNH_3^+ accounts for 80 ± 2% for all species, ruling out speciation differences as the primary factor for the observed effects.

Fig. 8b further explores adsorption behavior between Si nanoparticles and alkylamines *via* zeta potential measurements. Due to electrostatic attraction, RNH_3^+ species readily adsorbed onto the negatively charged Si surface, increasing the zeta potential [55]. Intriguingly, under equivalent protonated species concentration, longer-chain alkylamines exhibit stronger adsorption, as evidenced by progressively higher zeta potentials (**Fig. 8**b). At 10 mM, zeta potential increases slightly from -34 mV (C_1) to -20 mV (C_6). At 100 mM, this effect becomes more pronounced, shifting from -28 mV (C_1) to nearly neutral -1 mV (C_6). This enhanced adsorption capacity with increasing chain length likely plays a key role in modulating the CMP performance (**Figs. 2** and **3**), underscoring the critical influence of molecular architecture on surface interactions during Si CMP.

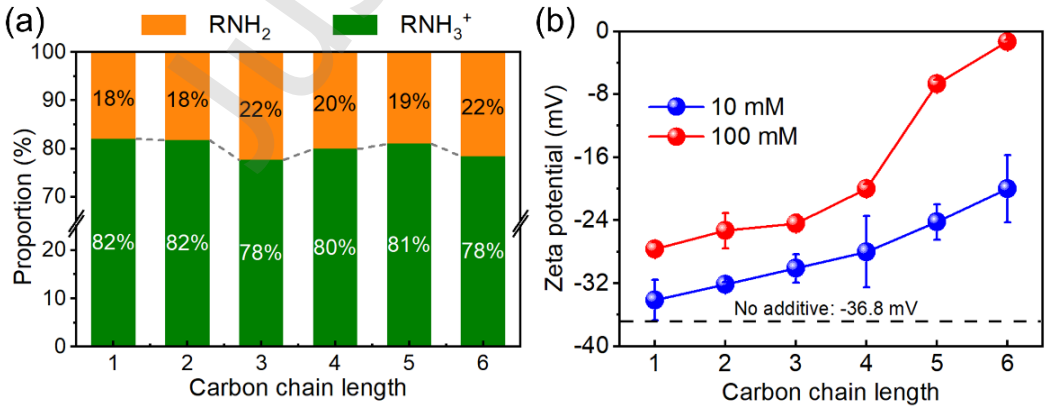

Fig. 8 (a) Calculated distribution diagram of the six alkylamine species in an aqueous solution at pH 10. R represents alkyl group with different carbon chain lengths. (b) Carbon chain length

and concentration effects of the alkylamines on the zeta potential of Si nanoparticles.

3.3 Characterization of chemical and mechanical properties of Si surfaces after etching by alkylamine-based solution

For further characterization, MA (C_1) and HA (C_6) were selected as representative short- and long-chain alkylamines, owing to their pronounced differences in polishing performance and adsorption behavior. XPS analysis of the Si surface (**Fig. 9**a) reveals no distinct N 1s peak in the absence of alkylamine. However, surfaces treated with alkylamines exhibit two peaks at 401.3 eV and 399.6 eV (**Fig. 9**b-e), corresponding to N–C and N–Si bonds, respectively [56, 57]. The atomic proportions of the N–C and N–Si components were obtained from peak deconvolution and are summarized in **Fig. 9**, indicating the chemical adsorption of alkylamines on the Si surface. The intensity of N 1s signals correlates with the extent of alkylamine adsorption, as supported by zeta potential results (**Fig. 8**b). Although long-chain alkylamines may lead to chemical residues due to chemical adsorption, this issue can generally be solved through standard industrial cleaning procedures without introducing significant additional complexity [33]. **Fig. 9**f–g displays the deconvoluted O 1s XPS spectra of the Si surfaces, revealing peaks at 531.8 eV and 532.5 eV, attributed to O^{2-} and OH^- species [58]. Compared to the original Si surface, the atomic proportions of the etched Si surface indicate that OH^- is the dominant species, suggesting enhanced surface hydroxylation induced by alkylamine adsorption. The deconvolution of Si 2p spectra of original surface reveals three peaks at 103.1 eV, 99.7 eV, and 99.1 eV, corresponding to suboxide Si_m–O_n (2m>n), Si $2p_{1/2}$, and Si $2p_{3/2}$, respectively (**Fig. 9**k) [59, 60]. Upon alkylamines treatment (**Fig. 9**i~o), a left peak with 102.5–

102.7 eV, assignable to O_x–Si–N_y compounds, with corresponding atomic ratios detailed in **Fig. 10** [61]. At 10 mM alkylamines concentration, the O_x–Si–N_y content is 5.9% for MA (C_1) and slightly higher (7.5%) for HA (C_6). When the concentration increases to 100 mM, the ratio increases sharply to 16.0% for MA (C_1) but decreases to 4.9% for HA (C_6). This contrast is attributed to the formation of a continuous HA-based film, which stabilizes the interfacial structure under mechanical loading [50], suppressing OH^- induced Si–Si bonds cleavage and thereby limiting O_x–Si–N_y formation [20].

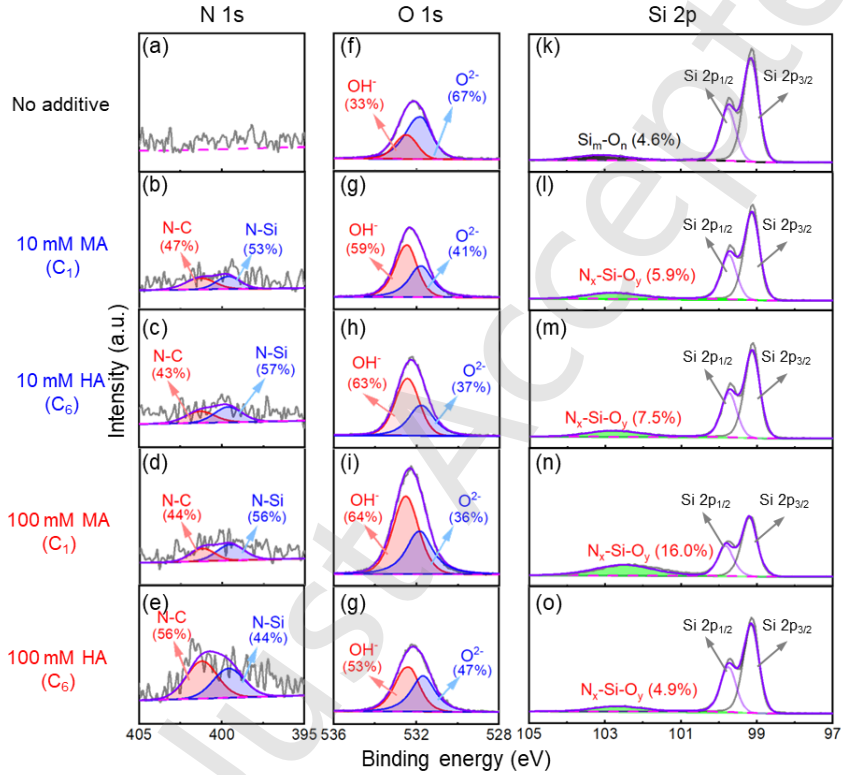

Fig. 9 XPS measurements on the original and etched Si surfaces. The etched surfaces were treated with the 10 mM and 100 mM solutions of short-chain (MA) and long-chain (HA) alkylamines. (a-e) N 1s, (f-g) O 1s, and (k-o) Si 2p XPS spectra.

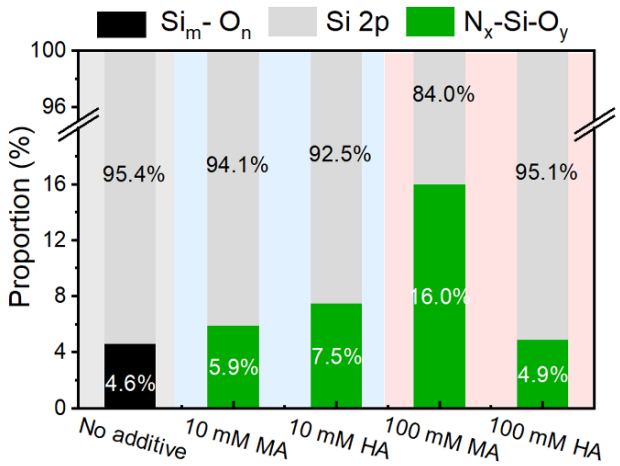

Fig. 10 Atomic proportion of Si_m–O_n, O_x–Si–N_y and Si determined by the XPS spectra in **Fig. 9**k-o.

The mechanical properties of the reaction layer formed on Si surface were evaluated by nanowear tests using a chemically inert diamond tip (**Fig. 11**a). Representative AFM topographies and corresponding cross-sectional profiles of scratches in **Fig. 11**b. The measured wear depth exhibited a consistent trend with the MRR (**Fig. 2**b) and the SER (**Fig. 6**b). As summarized in **Fig. 11**c, the wear depth and volume of the wear scratches on the etched Si surface without alkylamine reached 9.2 nm and 6.0×10^4 nm^3, respectively, which increased to 12.0 nm/6.7×10^4 nm^3 with the addition of 10 mM alkylamine. At 100 mM, the wear depth/volume on MA-etched surface exhibits a substantial increase to 18.8 nm/9.9×10^4 nm^3. This enhancement is attributed to intensified chemical reactions between the amine group and Si surface, facilitating the formation of mechanically weaker O_x–Si–N_y compounds that are more susceptible to mechanical removal. In contrast, a notable reduction to 7.9 nm/5.6×10^4 nm^3 was observed on HA-etched surface, likely due to the lower concentration of O_x–Si–N_y species and protective effect of the dense and uniform HA-based film. These results (**Figs. 10**

and **11**) underscore the significant impact of alkylamines chain length on both the chemical reactivity and mechanical stability of reaction layer. The interplay between interfacial chemistry and nanomechanical response plays a critical role in modulating the CMP performance of Si surfaces.

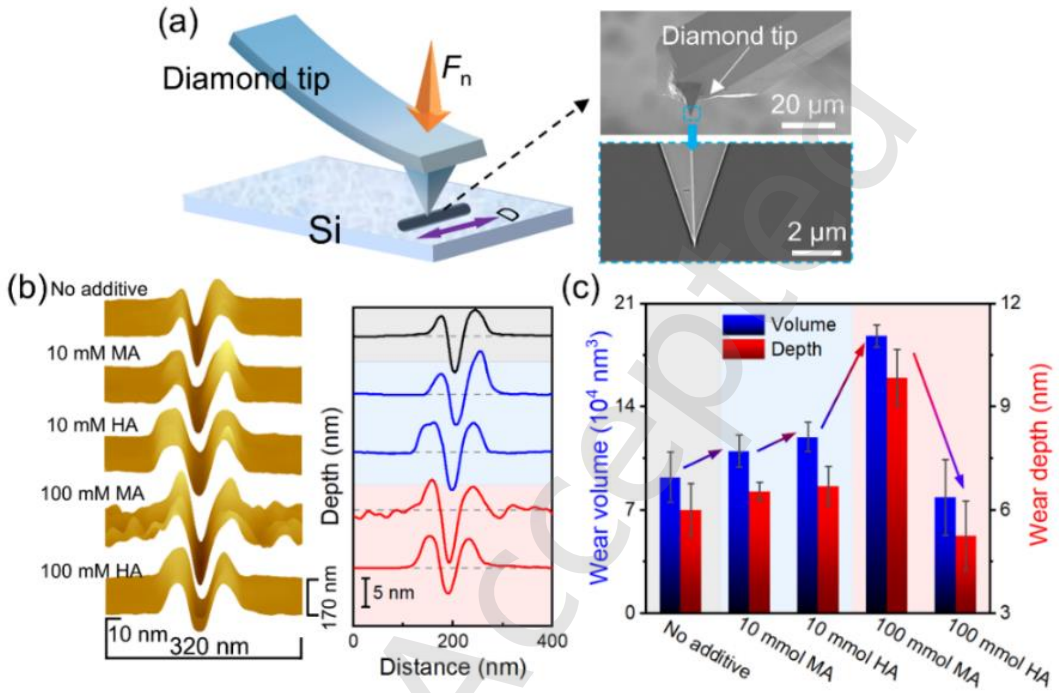

Fig. 11 Nanowear tests on the original and etched Si surfaces. (a) Schematic representation of the wear test on Si surface with a diamond tip. (b) AFM topographies and cross-sectional profiles of wear scratches formed on the surfaces by a cone shaped diamond tip. (c) Comparison of wear volume and depth of the wear scratches in (b).

3.4 Atomic-scale insights into the interfacial interaction mechanism between alkylamine and Si in CMP

To further elucidate the underlying mechanism by which the carbon chain length and concentration of alkylamine affect the CMP performance of Si, DFT calculations were performed to simulate the interaction between alkylamine and Si surface at atomic scale. The reaction process can be divided into three sequential steps: non-dissociative pre-adsorption,

chemical adsorption of alkylamine (N–H bond cleavage), and hydroxy substitution reaction (original H-terminated surface replaced by surface OH^- groups) (**Fig. 12**a). In reaction 1, alkylamine molecules are non-dissociative pre-adsorbed onto the Si surface, resulting in a ~11% reduction in the bond force constants of topmost layer Si–Si bonds compared to the initial configuration (**Fig. 12**b) [20]. This weakening is likely caused by charge redistribution induced by alkylamine adsorption, as evidenced by charge analysis results (**Fig. 13)** [50, 62]. In reaction 2, the amine groups undergo selective N–H bond dissociation, generating surface-bonded hydrogen species (right-side configurations). However, these intermediates are unstable under alkaline conditions and are prone to nucleophilic attack by water molecules [63]. This process triggers the subsequent Reaction 3, wherein hydrogen atoms on the Si surface are replaced with hydroxyl groups via a hydroxy substitution reaction [64]. Compared to Reaction 1, the configuration of the final state in Reaction 3 shows a reduced weakening effect of alkylamines on Si–Si bonds, as indicated by a ~4% rebound in the bond force constants (**Fig. 12**b).

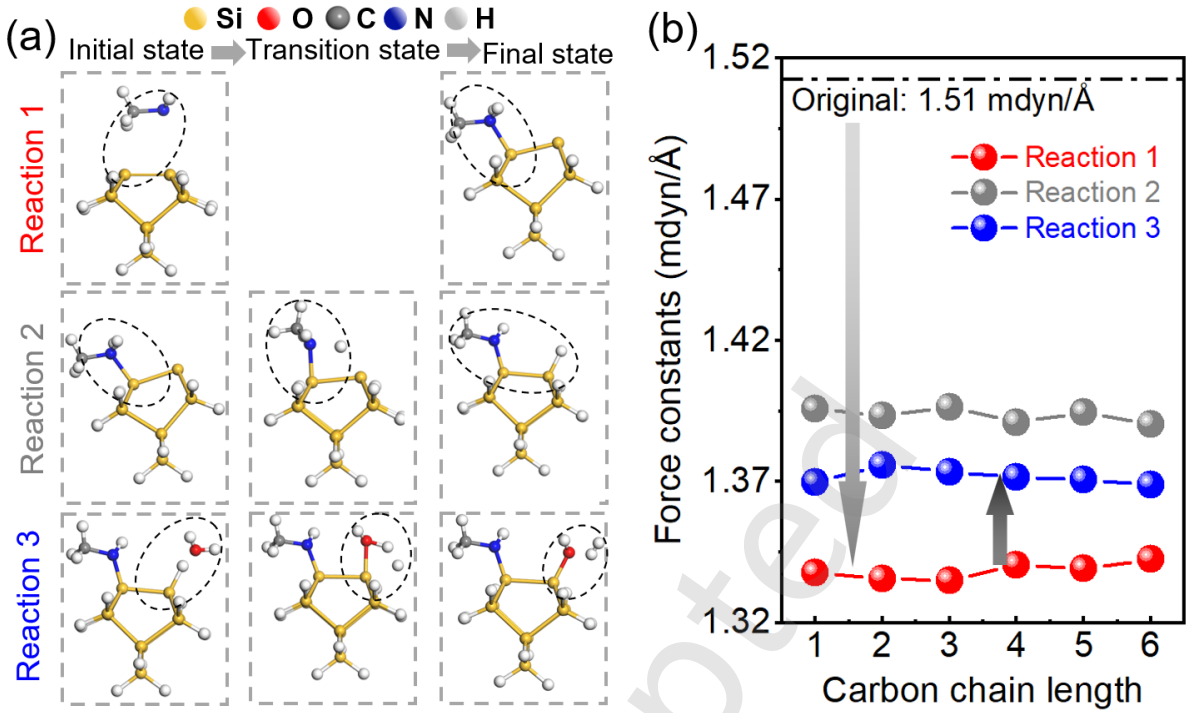

Fig. 12 Reaction process between alkylamines (MA) and Si. (a) Three sequential reactions between alkylamine and Si surface. (b) Si–Si bond force constants of final configurations as a function of carbon chain length in the three reaction processes.

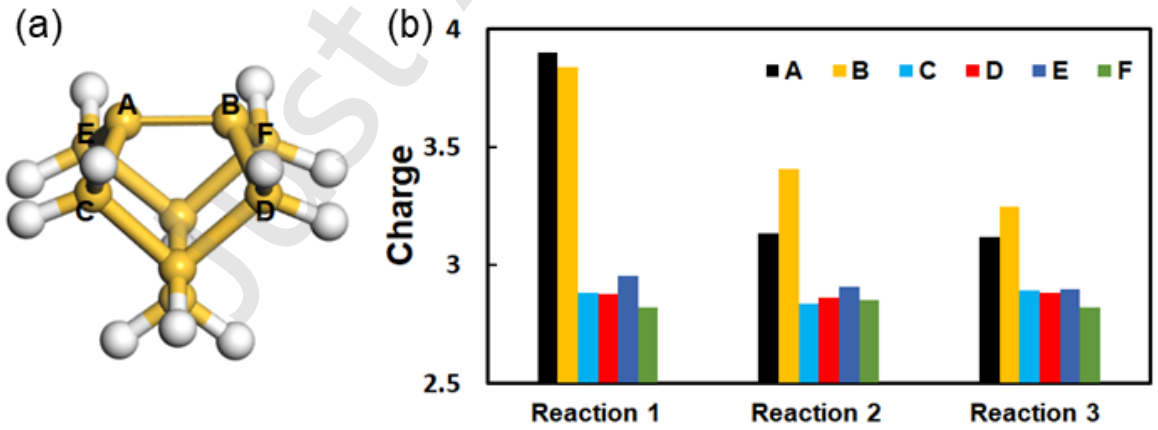

Fig. 13 Atomic charge distribution of Si cluster in the three reactions. (a) Schematic of geometric structure and atomic sites of the Si cluster. AB and CDEF represent surface and subsurface atoms, respectively. (b) Charge distribution data of the six atoms after the reaction.

The reaction system is sensitive to the energy barrier with both physical and chemical adsorption of alkylamine on the Si surface, which directly influence the reaction rate. Due to the negligible physisorption energy barrier (< 0.15 eV) for Reaction 1, the non-dissociative adsorption energy decreases significantly with increasing carbon chain length, suggesting that longer-chain alkylamines adsorber more readily onto the Si surface (**Fig. 14**a). A similar trend is observed in the chemical adsorption barriers (**Fig. 14**b), suggesting that longer-chain also promotes bond cleavage on the surface. This dual facilitation, enhanced physical and chemical adsorption, makes the reaction rate between longer-chain alkylamines and Si more susceptible to be dominated by Reaction 2 and Reaction 3, whereas the reaction involving short-chain alkylamines are more likely to be governed by Reaction 1.

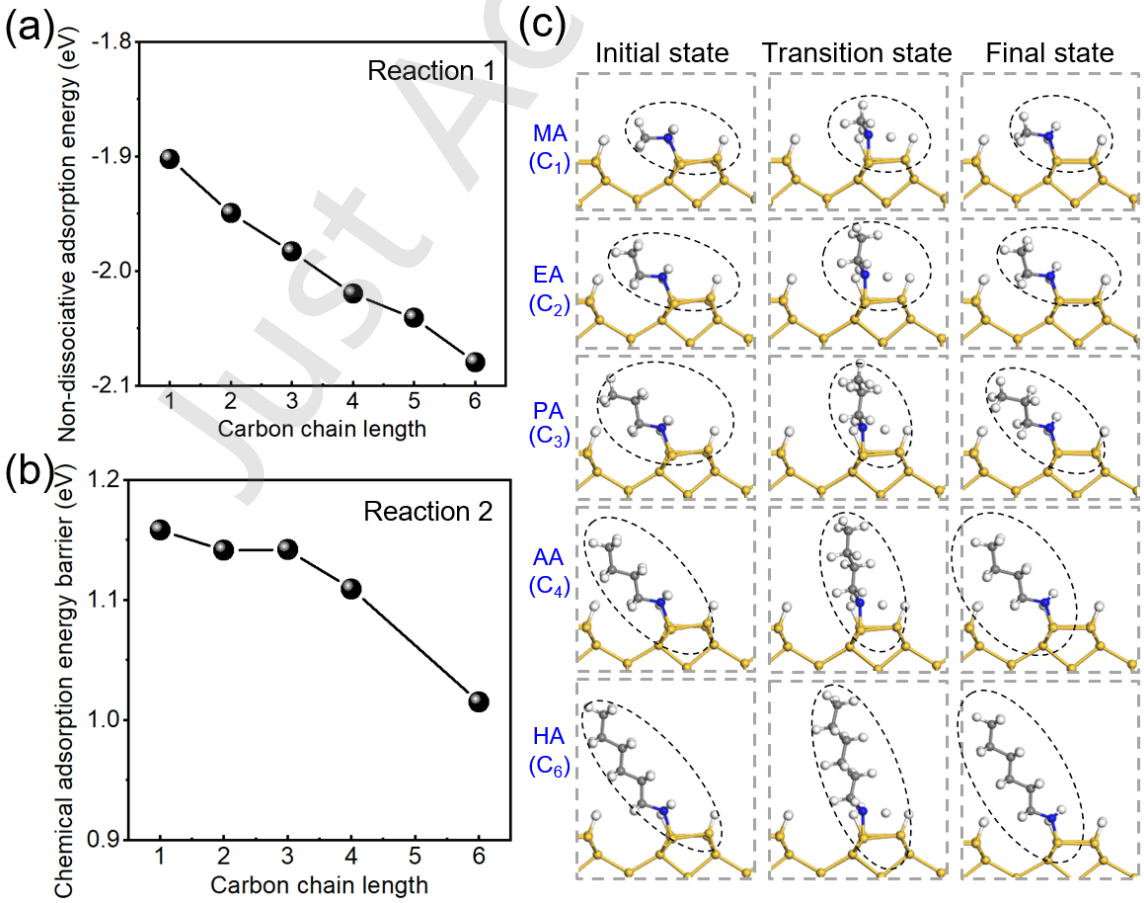

Fig. 14 (a) Non-dissociative pre-adsorption energy and (b) chemical adsorption energy barrier as a function of alkylamine chain length. (c) The reaction pathways between alkylamine and Si.

At low alkylamine concentration (e.g. 10 mM), the Si–Si bond weakening induced by longer-chain alkylamines, which are primarily governed by Reactions 2 and 3, is less pronounced than that caused by short-chain alkylamines dominated by Reaction 1. However, the significantly higher surface adsorption of long-chain species (**Fig. 14**a) compensates for this, thereby enhancing the MRR of Si. This mechanism likely explains the observed MRR increase from 306.1 nm/min for MA (C_1) to 369 nm/min for HA (C_6) at low alkylamine concentrations (**Fig. 2**c).

At high concentrations (e.g. 100 mM), the abundance of shorter-chain alkylamines results in greater adsorption and stronger Si–Si bond weakening via Reaction 1, promoting the formation and removal of the surface reaction layer and resulting in a higher MRR (e.g. MA, 555 nm/min). However, for long-chain alkylamines, two cooperative effects emerge: (1) the bond-weakening capability decreases markedly (**Fig. 12**b), and (2) the stronger adsorption promotes the formation of a continuous, uniform protective layer which shields the Si surface from external mechanical action (**Fig. 11**). The combination of these effects impedes both the formation and removal of the reaction layer, ultimately lowering the MRR (e.g. HA, 57.7 nm/min). Moreover, during CMP, the long-chain based protective layer preferentially shields the recessed areas of the Si surface from both chemical and mechanical actions. In contrast, protruding areas remain exposed and are selectively removed, enabling ultra-precision planarization (**Fig. 3**).

3.5 Underlying action mechanism of alkylamines with varying carbon chain length on CMP performance of Si

Based on the multiscale experimental results, a proposed mechanism illustrating how alkylamines affect the CMP performance of Si is presented in **Fig. 15**. The physical and dissociative adsorption energy barriers decrease with increasing carbon chain length (**Fig. 14**). Consequently, short-chain alkylamines exhibit weaker adsorption capacity but stronger Si–Si bonds weakening, whereas long-chain alkylamines adsorb more readily but exert a milder weakening effect (**Fig. 12**). Compared to slurries containing low concentrations of short chain alkylamines (**Fig. 15**a), surface adsorption on Si surface is slightly enhanced either by employing lower concentrations of long-chain alkylamines (**Fig. 15**b) or higher concentrations of short-chain alkylamines (**Fig. 15**c). In both cases, the number of Si–Si bonds weakened by amine groups increases, facilitating the formation of a mechanically fragile reaction layer composed of O_x–Si–N_y compounds (**Figs. 9** and **11**), thereby improving the MRR (**Fig. 2**). However, the introduction of high concentrations of longer-chain alkylamines into the slurry leads to a surface passivation effect, primarily due to the diminished bond-weakening capability and the formation of a near-saturation protective adsorption layer (**Fig. 8**b), which significantly impedes the formation and removal of the reaction layer (**Fig. 15**d). Moreover, the recessed areas of the Si surface are shielded from chemical aggressiveness and mechanical action by the protective layer, while the protruding regions remain exposed to mechanical action, resulting in their preferential removal in the polishing process. This selective removal enables efficient planarization of rough Si surfaces.

The chain-length-dependent bond weakening and absorption behaviors enable slurry to be designed with specific performance to meet the CMP requirements encountered in advanced chip manufacturing. For example, long-chain HA-based slurries are suitable for achieving atomic-level smooth surfaces required for lithography or ion implantation [52]; short-chain MA-based slurries can meet the demands of through-silicon-via CMP, delivering MRR exceeding 500 nm/min while obtaining a sub-nanometer rough surface [35, 65]. This suggests that slurry design can shift from empirical optimization to a more predictive strategy. Moreover, the alkylamine chain length serves as an effective bridge to modulate mechanical and chemical interactions in CMP, enabling controlled MRR and achieving atomic surface. This atomic mechanistic framework may provide useful insights for achieving atomic surfaces on other semiconductor materials (e.g. diamond, SiC and GaN), where obtaining such surfaces remains challenging due to the difficulty in controlling interfacial mechanochemistry during polishing.

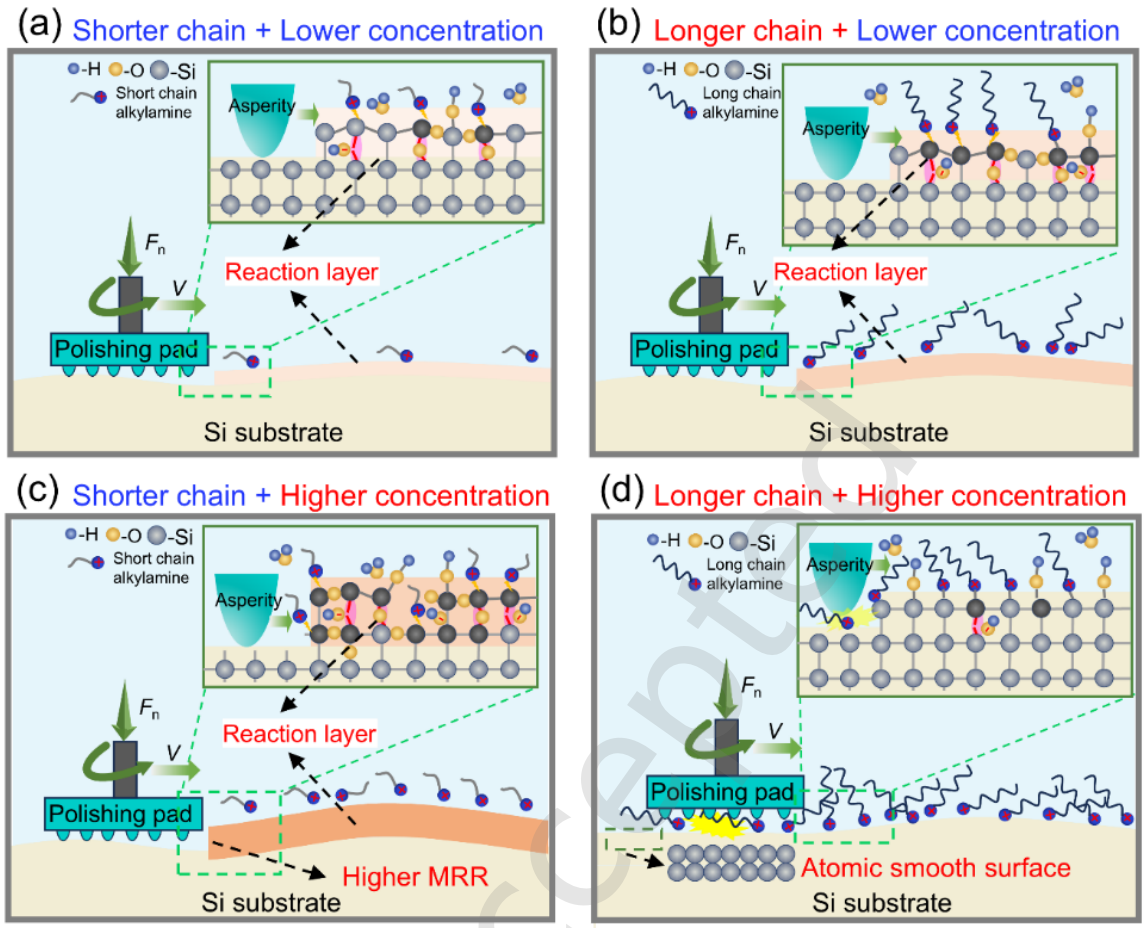

Fig. 15 Schematic representation of the CMP mechanism. Polishing of Si with shorter-chain alkylamines and longer-chain alkylamines at lower concentration (a-b) and higher concentration (c-d).

4. Conclusion

In this study, a series of alkylamines were introduced as key additives in the abrasive-free CMP slurries for Si. The underlying mechanism of molecular structure of alkylamines on CMP performance was systematically elucidated. The main conclusions are as follows:

(1) At a low alkylamine concentration (10 mM), the MRR of Si increases slightly with the carbon chain length. This enhancement is attributed to the reduced energy barriers for both physical and dissociative adsorption, which promote the adsorption of more long-chain

alkylamine molecules onto the Si surface. Consequently, this increased surface coverage leads to a greater number of weakened Si–Si bonds, facilitating the formation of a mechanically weakened reaction layer composed by O_x–Si–N_y compounds, thereby enhancing the MRR.

(2) At a high alkylamine concentration (100 mM), both the MRR and S_a of Si decrease significantly with increasing chain length. This behavior is attributed to two key factors: (i) the weakening effect of longer-chain alkylamines on Si–Si bonds is less pronounced compared to shorter-chain counterparts; (ii) near-saturation adsorption of long-chain alkylamines results in the formation of a continuous protective layer, which passivates the surface and inhibits both chemical attack and mechanical removal, ultimately reducing MRR and S_a.

(3) Our findings shift the mechanistic paradigm from conventional abrasive-involved interfacial interactions to abrasive-free, chemically driven, adsorption-controlled removal processes. This work fundamentally advances the understanding of CMP by identifying the dynamic equilibrium between adsorption strength and bond weakening as the key driving mechanism. This mechanistic understanding enables slurry design from empirical optimization toward a more predictive strategy, where molecular structure is deliberately tailored to meet specific CMP requirements in ICs. In particular, the chain-length-dependent interfacial mechanochemistry establishes a broadly applicable theoretical framework for CMP, extending beyond Si to materials such as diamond, SiC and GaN commonly used in advanced semiconductor manufacturing.

Declaration of Competing Interest

The authors declare that they have no known competing financial interests or personal relationships that could have appeared to influence the work reported in this paper.

Acknowledgments

The authors are grateful for the financial support from the National Key Research and Development Program of China-Young Scientist Program (2023YFB3405500), the National Natural Science Foundation of China (Nos. 52350411 and 52405217), Sichuan Science and Technology Program (Nos. 2023NSFSC1988 and 2025YFHZ0164), the Tribology Science Fund of the State Key Laboratory of Tribology in Advanced Equipment (No. SKLTKF24B08).

References

[1] Zhang Z Y, Liu J, Hu W, Zhang L Z, Xie W X, Liao L X, Chemical mechanical polishing for sapphire wafers using a developed slurry. *J Manuf Process* **62**: 762-771 (2021)

[2] Lei X F, Zhang Z Y, Zhou H X, Yang X F, Hu P F, He L H, Liu X Z, Cai H X, Pang Z H, Novel eco-friendly chemical mechanical polishing of aluminum alloy for achieving close atomic surface. *Wear* **578**: 206174 (2025)

[3] Liu J H, Pei Z J, Fisher G R, ELID grinding of silicon wafers: A literature review. *Int J Mach Tools Manuf* **47**(3): 529-536 (2007)

[4] Zhao F, Zhang Z Y, Zhou H X, Feng J Y, Deng X Q, Liu Z S, Meng F N, Shi C J, Novel full-scale model verified by atomic surface and developed composite microfiber and slurry polishing system. *Compos Part B-Eng* **283**: 111598 (2024)

[5] Dong L G, Zhang Z Y, Zhao F, Li Q Y, Zhou H X, Yang X F, Liu X Q, Guo J D, Zheng X, Atomic surface on a Ni alloy produced by novel green chemical mechanical polishing. *Tribol Int*: 110902 (2025)

[6] Yu Z B, Zhang Z Y, Zhao F, Hu J J, Zhong S C, Ren Z Y, Wang X R, Dai G Y, Weng Q, Review on advanced atomic-level polishing for single crystal diamond. *Surf Interfaces* **72**: 107443 (2025)

[7] Liu Z S, Zhang Z Y, Feng J Y, Yi X, Shi C J, Gu Y, Zhao F, Liu S H, Li J R, A novel atomic removal model for chemical mechanical polishing using developed mesoporous shell/core abrasives based on molecular dynamics. *Nanoscale* **16**(1): 85-96 (2024)

[8] He Y, Gorman S K, Keith D, Kranz L, Keizer J G, Simmons M Y, A two-qubit gate between phosphorus donor electrons in silicon. *Nature* **571**(7765): 371-375 (2019)

[9] Cao W, Bu H M, Vinet M, Cao M, Takagi S, Hwang S, Ghani T, Banerjee K, The future transistors.

Nature **620**(7974): 501-515 (2023)

[10] Wang D, Xie W X, Zhang Z Y, Wang J M, Shi C J, Meng F N, Zhuang X Y, Tong D Y, Cao C, Atomic surface of silicon wafers induced by grafted silica nanoparticles and sodium carbonate. *Appl Surf Sci* **664**: 160234 (2024)

[11] Yu Z B, Jia Z H, Liu W, Zhang Z Y, Zhao F, Fan C, Zhang H S, Lyv Y Q, Liu D D, Facet-dependent oxidative fabrication of diamond determined by operando scanning electron microscopy. *Nano Lett* **25**(13): 5391-5397 (2025)

[12] Yu Z B, Zhang Z Y, Zeng Z N, Fan C, Gu Y, Shi C J, Zhou H X, Meng F N, Feng J Y, Atomic surface of diamond induced by novel green photocatalytic chemical mechanical polishing with high material removal rate. *Int J Extreme Manuf* **7**(2): 025102 (2024)

[13] Zhao F, Zhang Z Y, Zhou H X, Chen L L, Hai K, Wu L W, Yu J H, Zhang Z F, Fan C, Unprecedented developed composite polishing system to achieve atomic surface integrating rough and fine polishing using a novel hyper-conjugated pad through controlling the temperature of a proposed green slurry. *Adv Compos Hybrid Mater* **8**(3): 1-18 (2025)

[14] Wang D, Liu L, Zhang Z Y, Peng Q B, Shi C J, Liu X Q, Liu X Y, Zhou H X, Wen W, Atomic-scale planarization surface of quartz glass induced by novel green chemical mechanical polishing using three ingredients. *Mater Today Sustainability* **25**: 100669 (2024)

[15] Zhao F, Zhang Z Y, Deng X Q, Feng J Y, Zhou H X, Liu Z S, Meng F N, Shi C J, Atomic surface achieved through a novel cross-scale model from macroscale to nanoscale. *Nanoscale* **16**(5): 2318-2336 (2024)

[16] Liu D D, Zhang Z Y, Zhou H X, Deng X Q, Shi C J, Meng F N, Yu Z B, Feng J Y, Angstrom surface on copper induced by novel green chemical mechanical polishing using ceria and silica composite

abrasives. *Appl Surf Sci* **640**: 158382 (2023)

[17] Dang S H, Xiao C, Zhang X Y, Li J, Wang Y, Qian L M, Chen L, Asynchronous mechanochemical atomic attrition behavior of heterogeneous polysilicon surface. *Wear* **570**: 205915 (2025)

[18] Wang Z Y, Liu P Z, Lee J Y, Lee H J, Kim H, Hwang H, An Y H, Kim T, Investigation of cleaning mechanisms for particle, metal ion, and organic contaminations in amorphous carbon post-CMP cleaning. *Appl Surf Sci*: 164803 (2025)

[19] Nguyen V T, Wait J, Nishi T, Hamada S, Himaya H, Seo J, Systematic root cause analysis of ceria-induced defects during chemical mechanical planarization and cleaning. *J Manuf Process* **127**: 27-34 (2024)

[20] Dandu P V, Peethala B, Penta N K, Babu S, Role of amines and amino acids in enhancing the removal rates of undoped and P-doped polysilicon films during chemical mechanical polishing. *Colloid Surface A* **366**(1-3): 68-73 (2010)

[21] Penta N K, Veera P D, Babu S, Charge density and pH effects on polycation adsorption on poly-Si, SiO_2, and Si_3N_4 films and impact on removal during chemical mechanical polishing. *ACS Appl Mater Interfaces* **3**(10): 4126-4132 (2011)

[22] Liu J W, Jiang L, Wu H Q, Zhong X, Qian L M, Performance of carboxyl groups in chemical mechanical polishing of GCr15 bearing steel: Effects of carbon chain length and pH. *Tribol Lett* **69**(4): 161 (2021)

[23] Zhang L C, Biddut A Q, Ali Y M, Dependence of pad performance on its texture in polishing mono-crystalline silicon wafers. *Int J Mech Sci* **52**(5): 657-662 (2010)

[24] Xiao C, Deng C B, Zhang P, Qian L M, Kim S H, Interplay between solution chemistry and mechanical activation in friction-induced material removal of silicon surface in aqueous solution.

Tribol Int **148**: 106319 (2020)

[25] Zhang Z y, Du Y F, Wang B, Wang Z G, Kang R K, Guo D M, Nanoscale wear layers on silicon wafers induced by mechanical chemical grinding. *Tribol Lett* **65**(4): 132 (2017)

[26] Lansbergen G P, Rahman R, Wellard C J, Woo I, Caro J, Collaert N, Biesemans S, Klimeck G, Hollenberg L C L, Rogge S, Gate-induced quantum-confinement transition of a single dopant atom in a silicon FinFET. *Nat Phys* **4**(8): 656-661 (2008)

[27] Chen L, Wen J L, Zhang P, Yu B J, Chen C, Ma T B, Lu X C, Kim S H, Qian L M, Nanomanufacturing of silicon surface with a single atomic layer precision via mechanochemical reactions. *Nat Commun* **9**(1): 1542 (2018)

[28] Cui X X, Zhang Z Y, Yu S Q, Chen X, Shi C J, Zhou H X, Meng F N, Yu J X, Wen W, Unprecedented atomic surface of silicon induced by environmentally friendly chemical mechanical polishing. *Nanoscale* **15**(21): 9304-9314 (2023)

[29] Xie W X, Zhang Z Y, Wang L, Cui X X, Yu S Q, Su H J, Wang S D, Chemical mechanical polishing of silicon wafers using developed uniformly dispersed colloidal silica in slurry. *J Manuf Process* **90**: 196-203 (2023)

[30] Guo J, Gong J, Shi P F, Xiao C, Jiang L, Chen L, Qian L M, Study on the polishing mechanism of pH-dependent tribochemical removal in CMP of CaF_2 crystal. *Tribol Int* **150**: 106370 (2020)

[31] Yu J X, Kim S H, Yu B J, Qian L M, Zhou Z R, Role of Tribochemistry in Nanowear of Single-Crystalline Silicon. *ACS Appl Mater Interfaces* **4**(3): 1585-1593 (2012)

[32] Wen J L, Ma T B, Zhang W W, Psofogiannakis G, van Duin A C T, Chen L, Qian L M, Hu Y Z, Lu X C, Atomic insight into tribochemical wear mechanism of silicon at the Si/SiO_2 interface in aqueous environment: Molecular dynamics simulations using ReaxFF reactive force field. *Appl*

Surf Sci **390**: 216-223 (2016)

[33] Zhang L M, Raghavan S, Weling M, Minimization of chemical-mechanical planarization (CMP) defects and post-CMP cleaning. *J Vac Sci Technol, B* **17**(5): 2248-2255 (1999)

[34] Dang S H, Xiao C, Li J, Jiang Y L, Franklin S E, Qian L M, Chen L, Achieving highly selective polishing of polysilicon over oxide and nitride films via ethylenediamine-modulated interfacial mechanochemistry. *J Manuf Process* **156**: 497-508 (2025)

[35] Penta N K, Veera P R D, Babu S V, Charge density and pH effects on polycation adsorption on poly-Si, SiO_2, and Si_3N_4 Films and impact on removal during chemical mechanical polishing. *ACS Appl Mater Interfaces* **3**(10): 4126-4132 (2011)

[36] Shayesteh H, Raji F, Kelishami A R, Influence of the alkyl chain length of surfactant on adsorption process: A case study. *Surf Interfaces* **22**: 100806 (2021)

[37] Basim G B, Vakarelski I U, Moudgil B M, Role of interaction forces in controlling the stability and polishing performance of CMP slurries. *J Colloid Interface Sci* **263**(2): 506-515 (2003)

[38] Zhang Z Y, Yan J W, Kuriyagawa T, Manufacturing technologies toward extreme precision. *Int J Extreme Manuf* **1**(2): 022001 (2019)

[39] Datta D, Rai H, Singh S, Srivastava M, Sharma R K, Gosvami N N, Nanoscale tribological aspects of chemical mechanical polishing: A review. *Appl Surf Sci Adv* **11**: 100286 (2022)

[40] You Y F, He Z W, Zhou J W, Qi Y H, Luo C, Enhanced ruthenium removal and superior surface quality via abrasive-Free chemical mechanical polishing using synergistic catalysis with the H_2O_2/PDS/FeIII-NTA System. *Small* **21**(30): 2410586 (2025)

[41] Delley B, An all-electron numerical method for solving the local density functional for polyatomic molecules. *J Chem Phys* **92**(1): 508-517 (1990)

[42] Perdew J P, Burke K, Ernzerhof M, Generalized gradient approximation made simple. *Phys Rev Lett* **77**(18): 3865 (1996)

[43] Andzelm J, Kölmel C, Klamt A, Incorporation of solvent effects into density functional calculations of molecular energies and geometries. *J Chem Phys* **103**(21): 9312-9320 (1995)

[44] Elstner M, Hobza P, Frauenheim T, Suhai S, Kaxiras E, Hydrogen bonding and stacking interactions of nucleic acid base pairs: A density-functional-theory based treatment. *J Chem Phys* **114**: 5149-5155 (2001)

[45] Grimme S, Accurate description of van der Waals complexes by density functional theory including empirical corrections. *J Comput Chem* **25**(12): 1463-1473 (2004)

[46] Halgren T A, Lipscomb W N, The synchronous-transit method for determining reaction pathways and locating molecular transition states. *Chem Phys Lett* **49**(2): 225-232 (1977)

[47] Tao Y W, Zou W L, Sethio D, Verma N, Qiu Y, Tian C, Cremer D, Kraka E, In situ measure of intrinsic bond strength in crystalline structures: local vibrational mode theory for periodic systems. *J Chem Theory Comput* **15**(3): 1761-1776 (2019)

[48] Tao Y W, Zou W L, Nanayakkara S, Kraka E, LModeA-nano: A PyMOL plugin for calculating bond strength in solids, surfaces, and molecules via local vibrational mode analysis. *J Chem Theory Comput* **18**(3): 1821-1837 (2022)

[49] Shoemaker J, Burggraf L W, Gordon M S, An ab initio cluster study of the structure of the Si(001) surface. *J Chem Phys* **112**(6): 2994-3005 (2000)

[50] Sun J, Jiang Y, Du S, Chen L, Francisco J S, Cui S, Huang Q, Qian L, Charge redistribution in mechanochemical reactions for solid interfaces. *Nano Lett* **24**(23): 6858-6864 (2024)

[51] Xu X, Kang S Y, Yamabe T, Nitridation of Si(100)-(2×1) Surface byNH3: A Quantum Chemical

Cluster Model Study. *Phys Rev Lett* **88**(7): (2002)

[52] Chan A B, Nguyen C T, Ko P K, Chan S T, Wong S S, Polished TFT's: surface roughness reduction and its correlation to device performance improvement. *IEEE Trans Electron Devices* **44**(3): 455-463 (1997)

[53] Haynes W M, *CRC handbook of chemistry and physics*. CRC press, 2016

[54] Christian G D, Dasgupta P K, Schug K A, *Analytical chemistry*. John Wiley & Sons, 2013

[55] Bae J Y, Han M H, Lee S J, Kim E S, Lee K, Lee G s, Park J H, Park J G, Silicon wafer CMP slurry using a hydrolysis reaction accelerator with an amine functional group remarkably enhances polishing rate. *Nanomaterials* **12**(21): 3893 (2022)

[56] Chen C W, Huang C C, Lin Y Y, Chen L C, Chen K H, The affinity of Si–N and Si–C bonding in amorphous silicon carbon nitride (a-SiCN) thin film. *Diamond Relat Mater* **14**(3-7): 1126-1130 (2005)

[57] Li X M, Yang S, Wu X F, Preparation of silicon carbide nitride films on Si substrate by pulsed high-energy density plasma. *J Univ Sci Technol Beijing Miner Metall Mater* **13**(3): 272-276 (2006)

[58] Zou J L, Dai Y, Pan K, Jiang B J, Tian C G, Tian G H, Zhou W, Wang L, Wang X, Fu H G, Recovery of silicon from sewage sludge for production of high-purity nano-SiO_2. *Chemosphere* **90**(8): 2332-2339 (2013)

[59] Ulgut B, Suzer S, XPS studies of SiO_2/Si system under external bias. *J Phys Chem B* **107**(13): 2939-2943 (2003)

[60] Barr T L, An XPS study of Si as it occurs in adsorbents, catalysts, and thin films. *Appl Surf Sci* **15**(1-4): 1-35 (1983)

[61] Dong H, Chen K, Zhang P, Li W, Xu J, Ma Z, Sun Z, Liu Z, The role of Nx–Si–Oy bonding

configuration in acquiring strong blue to red photoluminescence from amorphous SiNxOy film. *Can J Phys* **92**(7/8): 602-605 (2014)

[62] Lu Y Y, Xiao C, Jiang Y L, Tang C, Chen L, Sun J H, Qian L M, Nanoscale wear triggered by stress-driven electron transfer. *Nano Lett* **23**(19): 8842-8849 (2023)

[63] Gräf D, Grundner M, Schulz R, Reaction of water with hydrofluoric acid treated silicon (111) and (100) surfaces. *J Vac Sci Technol A* **7**(3): 808-813 (1989)

[64] Yang J J, Wang E G, Reaction of water on silica surfaces. *Curr Opin Solid State Mater Sci* **10**(1): 33-39 (2006)

[65] Veera P D, Natarajan A, Hegde S, Babu S, Selective polishing of polysilicon during fabrication of microelectromechanical systems devices. *J Electrochem Soc* **156**(6): H487 (2009)

Shehui DANG. He received his bachelor's degree in mechanical engineering in 2021 from Dalian Jiaotong University, China. He is currently a Ph.D. candidate in mechanical engineering at Southwest Jiaotong University, China. His research interest includes chemical mechanical polishing and nanotribology.

Lei CHEN. He is a professor of mechanical engineering at Southwest Jiaotong University, China. He received his Ph.D. degree from Southwest Jiaotong University in 2013. He acted as a visiting scholar from 2016 to 2017 in The Pennsylvania State University, USA. He has a background in mechanical engineering and surface science. His current research interest includes atomic-level polishing, atomic-level modification. He can be reached at chenlei@swjtu.edu.cn.